Vol.46 No.5　2022

Journal

広告　◇東英工業株式会社

JOURNAL OF THE MAGNETICS SOCIETY OF JAPAN

Vol.46 No.5 **2022**

TOEI

世界初！
高温超電導型VSM

新製品

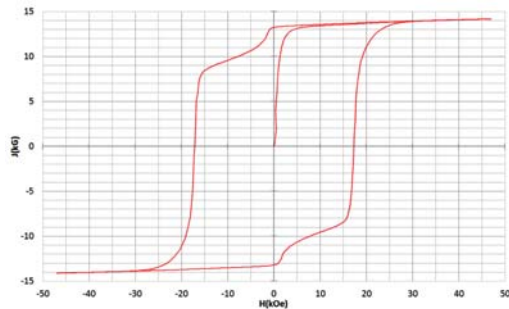世界初*、高温超電導マグネットをVSMに採用することで
測定速度 当社従来機1/20を実現。
0.5mm cube磁石のBr, HcJ高精度測定が可能と
なりました。
*2014年7月 東英工業調べ

測定結果例

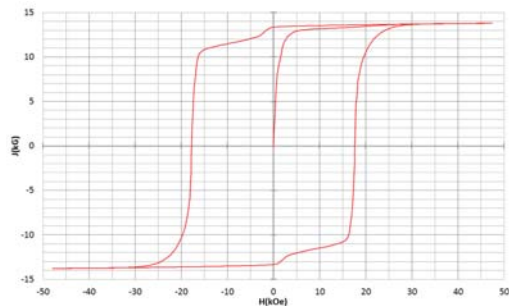### 高温超電導VSMによるNdFeB（sint.）0.5mm cube BHカーブ

磁化測定レンジ：0.2emu
Br = 13.2kG   HcJ = 17.2kOe

高温超電導VSMによるNdFeB（sint.）1mm cube BHカーブ

磁化測定レンジ：2emu
Br = 13.3kG   HcJ = 17.7kOe

高温超電導VSMによるNdFeB（sint.）4mm cube BHカーブ
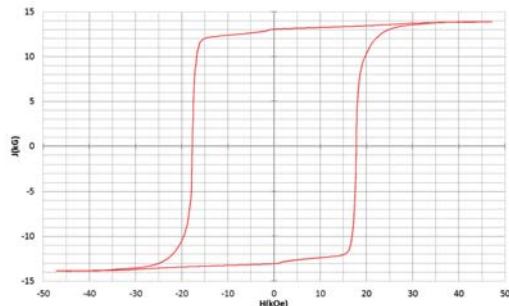
磁化測定レンジ：100emu
Br = 13.1kG   HcJ = 17.8kOe

高速測定を実現

高温超電導マグネット採用により、高速測定を
実現しました。Hmax＝5Tesla, Full Loop測定が
2分で可能です。
（当社従来機：Full Loop測定 40分）

小試料のBr,HcJ高精度測定

0.5mm cube磁石のBr,HcJ高精度測定ができ、
表面改質領域を切り出しBr,HcJの強度分布等、
微小変化量の比較測定が可能です。
また、試料の加工劣化の比較測定が可能です。

試料温度可変測定

－50℃～＋200℃温度可変UNIT（オプション）

磁界発生部の小型化

マグネットシステム部寸法：0.8m×0.3m×0.3m

TOEI 東英工業株式会社

http://www.toeikogyo.co.jp

〒194-0035 東京都町田市忠生1-8-13
TEL：042-791-1211 FAX：042-792-0490
E-mail : sales@toeikogyo.co.jp

Journal of the Magnetics Society of Japan
Vol. 46, No. 5

CONTENTS

<Paper>

Interpretation of Kronmüller formula using Ginzburg-Landau theory

C. Mitsumata and M. Kotsugi

Tokyo University of Science, *6-3-1, Niijuku, Katsushika, Tokyo, Japan 125-8585*

The Kronmüller formula is used to qualitatively explain the coercivity of permanent magnets. Such simple expressions are useful for understanding the elements that influence the coercivity. This study attempts to derive Kronmüller formula within the framework of the Ginzburg-Landau theory. The results revealed that the coercivity of the magnetic material was defined by the slope of the free energy landscape. The reduction parameter α for the magnetic anisotropy field H_k in the Kronmüller formula depends on the functional form representing the free energy landscape that changes with the magnetization process of the material, and it is shown that $\alpha < 1$ under the condition of absolute zero temperature $T = 0$. Furthermore, it was revealed that α depends on the entropy of the system and that it may show a larger reduction rate at a finite temperature $T \neq 0$. Thus, it is important to acquire the free energy landscape and clarify the order parameter dependence of entropy in the magnetization process of the magnetic material.

Key words: free energy, entropy, energy landscape, coercivity, magnetization process, permanent magnet, hard magnet

1   Introduction

The Kronmüller formula has been used to qualitatively explain the coercivity of permanent magnets. This simple expression is useful for understanding the elements that influence coercivity. The Kronmüller formula is shown below.

$$H_c = \alpha H_k - N_d M_s \qquad (1)$$

where H_c, H_k, N_d, and M_s are the coercivity, magnetic anisotropy field, demagnetizing coefficient, and saturation magnetization, respectively. This suggests that the coercivity can be explained by the magnetic anisotropy field and demagnetizing field. In particular, for the influence of the magnetic anisotropy field, the existence of the reduction coefficient ($0 < \alpha < 1$) shows the difficulty of the coercivity analysis.

The parameter α in Eq. (1) has been discussed in Kronmüller's theoretical model analysis[1,2] and in an experimental study by Hirosawa *et al.*[3]. However, the determination mechanism remains unclear, and further analysis is necessary to elucidate the coercivity mechanism.

Here, the determination principle of α in Eq. (1) is discussed using the Ginzburg-Landau theory[4]. A coercivity analysis of permanent magnets using the Ginzburg-Landau theory has previously been attempted[5–7]. However, a unified interpretation by comparison with the Kromüller formula has not yet been obtained. In recent years, the analysis of the energy landscape of permanent magnets[8] has been progressing, and expectations are rising for attempts to discuss coercivity from the perspective of free energy[9,10]. Therefore, in this study, the role of the energy landscape in the coercivity mechanism is clarified, and the effect of the coefficient in the expression of the Kronmüller formula is considered. In addition, the temperature dependence of the reduction parameter, α, is discussed.

Corresponding author: C. Mitsumata (mitsumata@rs.tus.ac.jp)

2   Derivation of Kronmüller formula

2.1   Simultaneous magnetization rotation model

In the Ginzburg-Landau theory, the free energy of the system is a function of the order parameter and the ordered state where the minimum condition of energies is determined to realize the stable state of the system. In magnetic materials, the order parameter is described by the magnetization state of the system, and the free energy density f is a function of the magnetization M.

Here, the order parameter represents an array in which the magnetization is $M^+ > 0$ or $M^- < 0$ in the local region. In the whole system, $M = M^+ + M^-$ describes the magnetization value and the array state of the system at the same time. Magnetization as an order parameter is different from the order of atomic arrangement. Even if the magnetization M is the same, the magnetization arrangement in the local region may be different, which corresponds to the magnetic domain structure. However, the single variable Landau theory in magnetic materials is a kind of mean field theory, and it is considered that the magnetization process of the system follows different energy landscapes when the magnetization M is equal and the magnetic domain structure is different. Information on different magnetic domain structures is an index that describes the diversity of the magnetization arrangement, and is reflected not in the difference in the order parameter but in the entropy corresponding to the certain order variable.

In addition, there is a definition that the order parameter in Landau theory expresses the anisotropy of the system. Therefore, when a directed line segment such as a magnetization vector is used as a variable of the scalar quantity, the system is described by the projection component in a certain direction and the entropy depending on such direction. For example, if the saturation state of the magnetization inside the material is $M_z = \pm M_s$, all the magnetizations in the local region are aligned in one direction. There is only one magnetization array that realizes those in each
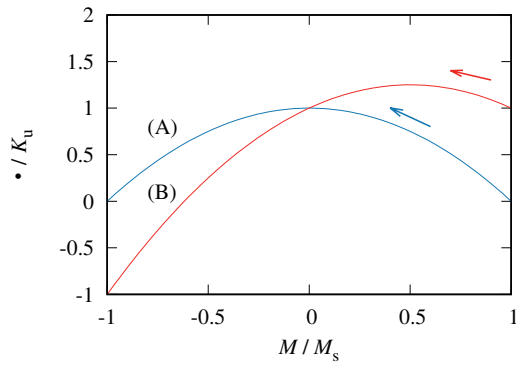
Fig. 1 Methodology for magnetization reversal on energy landscape within Ginzburg-Landau theory. (A) energy landscape of uni-axial magneitc anisotropy without an applied field, (B) under influence of an applied field.

case of positive and negative, and the entropy of the corresponding system is $S = 0$. In the case of a simultaneous rotation model, arbitrary M_x and M_y are accompanied in the magnetization reversal process from $M_z = +M_s$ to $M_z = -M_s$. All magnetizations are in the same direction and have a high degree of regularity, but deviations from a particular direction indicate a decrease in system anisotropy. Thus, using the polar coordinate representation, the entropy increases to $S = \log(1 + \int \sin\theta \cos\phi d\phi)$. Therefore, in this study, it is possible to describe the free energy by using the scalar quantity magnetization M as an order parameter.

Because the Kronmüller formula does not explicitly include a variable of temperature T, we first consider that the free energy density consists of only the term of magnetic energy density ε as the condition of $T = 0$.

$$\varepsilon(M) = K_u\left(1 - \frac{M^2}{M_s^2}\right) + \frac{1}{2}N_d M^2 \qquad (2)$$

K_u is the uniaxial magnetic anisotropy constant, N_d is the demagnetizing field coefficient, M is the magnetization, and M_s is the saturation magnetization. Equation (2) presents an expression that considers only the magnetic anisotropy energy and demagnetizing field energy.

Figure 1 shows the concept of magnetization reversal within the framework of the Ginzburg-Landau theory. Here, we consider simultaneous rotation as the magnetization process. Equation (2) forms the energy barrier required for magnetization reversal, and curve (A) shows the energy landscape without an applied magnetic field. The magnetization from the positive state ($M/M_s = 1$) is reversed to the negative state ($M/M_s = -1$) by overcoming the energy barrier, as indicated by the arrow. This is because the lowest energy state is $M/M_s = \pm1$. When an external magnetic field ($H_{app} < 0$) is applied to the system, the energy landscape, as shown in curve (B), changes owing to the influence of Zeeman energy. Thus, the energy barrier to be overcome from the state of $M/M_s = 1$ becomes smaller, as indicated by the arrow.

If the absolute value of the external magnetic field increases, the minimum state of energy existing at $M/M_s = 1$ disappears, and the magnetization state is inverted to $M/M_s = -1$ along the slope of the energy landscape. To summarize the above discussion, for magnetization reversal from positive to negative, the absence of a stable energy state in the region of $M > 0$ indicates the magnetization reversal condition, and the energy landscape becomes $\varepsilon' = \varepsilon - H_{app}M$ which is the addition of Zeeman energy in Eq. (2). That is,

$$\frac{\partial\varepsilon'}{\partial M} = -\frac{2K_u M}{M_s^2} + N_d M - H_{app} \geq 0 \qquad (3)$$

This is consistent with the monotonically increasing function of the energy landscape in the $M > 0$ region. In addition, because the result of differentiating the energy density ε' with the magnetization M indicates an effective magnetic field, Eq. (3) compares the magnitudes of magnetic fields. Therefore, the condition that the external magnetic field $H_{app} < 0$ required for magnetization reversal is satisfied is calculated as follows by the transformation of Eq. (3).

$$\left(-\frac{2K_u M}{M_s^2} + N_d M\right)_{min.} \geq H_{app} \qquad (4)$$

When the maximum $H_{app} < 0$ that satisfies the condition of Eq. (4) is applied to the system, the stable point on the energy landscape in the region of $M > 0$ disappears, and magnetization reversal occurs, that is, Eq. (4) describes the coercivity of magnetic materials. Because the permanent magnet satisfies the relationship $2K_u/M_s^2 > N_d$, the minimum value on the left-hand side of Eq. (4) is obtained when $M = M_s$. Corresponding conditional equation is as follows:

$$-H_c = -H_k + N_d M_s \qquad (5)$$

Here, the magnetization process of the system is assumed as simultaneous rotation: therefore, the Kronmüller formula for $\alpha = 1$ is obtained.

The presence of the reduction parameter $0 < \alpha < 1$ in Eq. (1) indicates a decrease in the coercivity. Therefore, in this analysis, there are two possibilities: the energy barrier is low, or the magnetic order has already climbed halfway through the energy barrier. The change in the magnetic anisotropy constant K_u is reflected in the change in H_k; therefore, it is irrelevant for the determination of α. The magnetostatic energy, as the second term in Eq. (2), can also be included in Eq. (4) as a coefficient for M^2. Among the above possibilities, it is speculated that the state of the system rising halfway through the energy barrier influences α. It should be noted that the change in the arrival point on the energy landscape means that the order parameter M also needs to change at the same time. Considering that irrationality occurs in the simultaneous rotation described by Eq. (2), and the possibility that the stable state of the system can be described by the order parameter $M \neq M_s$, it is necessary to have a discussion that reflects the influence of the multi-domain structure (non-uniformity of magnetization distribution). Even with an actual magnet material,

the squareness $\sigma = M_r/M_s$ (M_r is the remanent magnetization) shows that $\sigma < 1$, and the multi-domain structure exists stably under the condition of no external magnetic field ($H_{app} = 0$).

2.2 Multi-domain model

For non-uniform distribution of magnetization, the magnetization as an order parameter takes the value of $M < M_s$. With this in mind, we will reconsider the energy landscape. The requirements for the composition of the energy landscape are as follows.

- The energy landscape under no-magnetic-field conditions is symmetric with respect to $M = 0$.
- The saddle point of the energy barrier is formed under the condition of order parameter $M = 0$, and the demagnetization state is metastable.
- The magnetic domain structure of the residual magnetization state, $M_r = \sigma M_s (0 < \sigma < 1)$, forms a stable point.

Rewriting these required conditions,

$$\varepsilon(-M) = \varepsilon(M) \tag{6}$$

$$\left(\frac{\partial \varepsilon}{\partial M}\right)_{M=0} = 0, \quad \left(\frac{\partial^2 \varepsilon}{\partial M^2}\right)_{M\sim 0} \leq 0 \tag{7}$$

$$\left(\frac{\partial \varepsilon}{\partial M}\right)_{M=M_r} = 0, \quad \left(\frac{\partial^2 \varepsilon}{\partial M^2}\right)_{M\sim M_r} \geq 0 \tag{8}$$

However, it is assumed that there is no sudden change in the magnetic domain structure near stable and metastable points. Based on the conditions in Eq. (7) and Eq. (8), where the double derivative of the energy landscape function $\varepsilon(M)$ changes sign in the range of $0 < M < M_r$, $\varepsilon(M)$ is a function with at least one inflection point in the range of $0 < M < M_r$. The order parameter that gives this inflection point is defined as M_c. Simultaneously, considering the sign condition of the double derivative of $\varepsilon(M)$, the derivative $\partial \varepsilon/\partial M$ has the minimum value that is $(\partial \varepsilon/\partial M)_{M=M_c}$, while satisfying the condition of $(\partial \varepsilon/\partial M < 0)$ in the range of $0 < M < M_r$. This is because at $M = 0$, starting from $\partial \varepsilon/\partial M = 0$, the derivative becomes negative as M increases. When it reaches M_r beyond the inflection point, it returns to $\partial \varepsilon/\partial M = 0$. Therefore, there is always a negative minimum value in this section. Consequently, it is possible to calculate the coercivity of the energy landscape expressing the multi-domain structure using the same procedure as in the case of simultaneous rotation.

$$-H_c = \left(\frac{\partial \varepsilon}{\partial M}\right)_{M=M_c} \tag{9}$$

However, Eq. (9) is a conditional expression in the range $0 < M_c < M_s$, and in $-M_s < M_c < 0$, the sign on the left-hand side of the equation is inverted.

Innumerable functions satisfy the conditions in Eq. (6) to Eq. (8). Among them, the function that is differentially continuous in the range $-M_s \leq M \leq M_s$ and can be described by the lowest order of M is a quartic function. When the order of M increases,
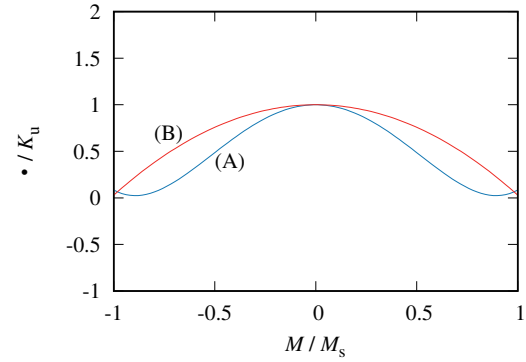
Fig. 2 Energy landscape comparison. (A) a quartic function representing the non-uniform magnetization distribution, (B) a quadratic function representing the simultaneous magnetization rotation.

the rate of change of the derivative $\partial \varepsilon/\partial M$ increases, and thus the coercivity H_c of Eq. (9) tends to increase[*1]. Therefore, the framework of the Ginzburg-Landau theory using the quartic function of M can be calculated to guarantee the minimum value of the coercivity. Moreover, the condition of differential continuity is a requirement of the conservation law of magnetic energy.

The energy landscape of the quartic function given by above conditions is shown below.

$$\varepsilon(M) = \frac{K_u}{\sigma^4 M_s^4} M^4 - \left(\frac{2K_u}{\sigma^2 M_s^2} - \frac{N_d}{2}\right) M^2 + K_u \tag{10}$$

As mentioned above, the order parameter represents the magnetization array and the projected component of the magnetization vector. Therefore, it is possible to consider the magnetic anisotropy energy due to the rotation of the magnetization in the magnetization process. Strictly speaking, when magnetization rotation occurs in the local region, the height of the energy barrier against magnetization reversal is considered to be smaller than K_u due to the influence of the magnetic domain structure. However, here it is approximated that the saddle point of the energy landscape is determined by K_u for direct comparison with the simultaneous rotation. That is, Eq. (10) assumed the maximum value of the possible energy barrier. Also, as shown in Fig. 2, the constant term K_u shifts the reference, so that it can be easily compared with the energy barrier of the simultaneous rotation model. Because the expression of the coercivity is given by the derivative of the energy landscape, there is no influence of the constant term on the analysis. For comparison, the energy landscapes in Eq. (10) and Eq. (2) are shown in Fig.2. (A) shows the case of the quartic equation and (B) represents the case of a quadratic equation. Here, for simplicity, the demagnetizing field coefficient $N_d = 1/3$ is used assuming a sphere as the material shape, where the demagnetizing field distribution inside the ma-

---

[*1] Assume that the height of the energy barrier at $M = 0$ is invariant in the cases of quadratic and quartic functions.

terial becomes uniform. In addition, function (A) is displayed under the condition that the squareness is $\sigma = 0.9$. The magnetization states that satisfy the respective minimum energy values are $M = \pm M_r = \pm\sigma M_s$ in case (A) and $M = \pm M_s$ in case (B).

To determine the coercivity from the energy landscape in Eq. (10). The inflection point is,

$$M_c^2 = \frac{\sigma^2 M_s^2}{3} - \frac{N_d \sigma^4 M_s^4}{12 K_u} \tag{11}$$

Substituting the magnetization showing the inflection point into the slope of the energy landscape.

$$\left(\frac{\partial \varepsilon}{\partial M}\right)_{M=M_c} = \left[\frac{4K_u}{\sigma^4 M_s^4} M_c^2 - 2\left(\frac{2K_u}{\sigma^2 M_s^2} - \frac{N_d}{2}\right)\right] M_c$$

$$-H_c = \sqrt{\frac{2H_k - \sigma^2 N_d M_s}{6H_k}} \left(-\frac{4}{3\sigma} H_k + \frac{2\sigma}{3} N_d M_s\right) \tag{12}$$

Because it is difficult to understand the square root coefficient, the coefficients of H_k and M_s are numerically approximated by parameters that imitate NdFeB magnets. Here, it is assumed that $\sigma = 0.9$. That is,

$$H_c = 0.84 H_k - 0.34 N_d M_s \tag{13}$$

From the Ginzburg-Landau theory, by evaluating the energy landscape, it becames clear that a reduction factor ($\alpha < 1$) that inevitably becomes $H_c < H_k$ can be obtained owing to the nonuniformity of magnetization.

The effect of the squareness σ is even more interesting. Comparing the coefficient terms proportional to H_k in Eq. (1) and Eq. (12).

$$\alpha = \frac{4}{3\sigma} \sqrt{\frac{2H_k - \sigma^2 N_d M_s}{6H_k}} \tag{14}$$

As shown, the reduction factor α is a function of σ. There are various possible reasons for $\sigma \neq 1$, but the dispersion of the magnetic anisotropy in the material is a factor that has a significant effect. Because uniaxial magnetic anisotropy is assumed here, it is not possible to discuss the case in which the dispersion of magnetic anisotropy is large. However, in the range where the average magnetic anisotropy $\overline{K}_u$ can be approximated as $\overline{K}_u \sim K_u$, α tends to decrease as σ increases [11]. That is, a seemingly contradictory result is derived in that the coercivity decreases as the degree of orientation of the crystal axis increases, which defines the average magnetic anisotropy. This result emphasizes the importance of discussing energy landscapes in the coercivity mechanism, as the energy landscape for magnetization reversal changes owing to the influence of the magnetization process.

3 Effect of entropy

In the previous section, we discussed the energy landscape when $T = 0$, and the effect of entropy was not considered. In Ginzburg-Landau theory, the stable state of the system with respect to the order parameter can be discussed using the free energy density f with the addition of the entropy term. Here, we redefine the free energy landscape, including the entropy effect.

$$f(M) = \varepsilon(M) - \frac{k_B T S(M)}{V} \tag{15}$$

where k_B is Bolzumann's constant, T is the temperature, S is the entropy of the system, and V is the volume of the system. Because S counts the degrees of freedom of the magnetization array, it is expressed as a function of the order parameter M only. In complex systems, such as magnet materials, it is difficult to precisely calculate S. Therefore, to understanding the coercivity mechanism qualitatively, a simple function that allows the function f to be calculated is introduced below.

In the discussion of magnetization reversal, the magnetization state is separated into regions with $M > 0$ or $M < 0$, and this region distribution forms a magnetic domain structure. Under conditions of strong uniaxial anisotropy, this assumption is considered a good approximation of the magnetic domain structure in permanent magnets. Considering that the positive and negative of the magnetization in the minute region represents the state of the magnetization array, the probability state density of the magnetization $P(M)$ can be expressed by the binomial distribution function.

$$P(M) = {}_n C_k p^k (1 - p)^{n-k} \tag{16}$$

where the coefficient ${}_n C_k$ is a combination that selects k elements from an array of n, and the probability p that determines the positive or negative magnetization is $p = 1/2$ [*2]. This is consistent with the method used to count the number of states in the Ising spin.

As the number of minute regions representing the magnetic domain structure is innumerable, the binomial distribution function expressing the stochastic density of states can be approximated by a Gaussian function representing the normal distribution.

$$P(M) = \sqrt{\frac{\phi}{\pi}} \exp\left(-\phi \frac{M^2}{M_s^2} + \phi\right) \tag{17}$$

Here, the average value of the magnetized states, $\overline{M}$, is $\overline{M} = 0$, and parameter ϕ in the probability state density function with M is a valid constant in the temperature range $0 \leq T < T_c$ (T_c is the Curie temperature). Meanwhile, $P(M)$ becomes a delta function $\delta(M)$ at $T \geq T_c$. In Eq. (17), the constant term in the exponential function guarantees that the number of states is only 1, where an ideal saturation state is $M = M_s$ or $M = -M_s$. In addition, ϕ is a constant that changes depending on the magnetization process, and as ϕ increases, the rate of change in the stochastic density of states with respect to the magnetization change of $M_s \to 0$ increases. Qualitatively, ϕ tends to be small with respect to the change in magnetization due to domain wall motion,

---

[*2] Strictly speaking, the probability of magnetization reversal depends on the magnetic domain structure, that is $p = 1/2 \pm \delta$. Here, it is assumed that the average of the reversal probabilities in all cases becomes $p = 1/2$, and that the ratio of exchange energy in the height of the energy barrier is small, thus it is set as $\delta \ll 1$.
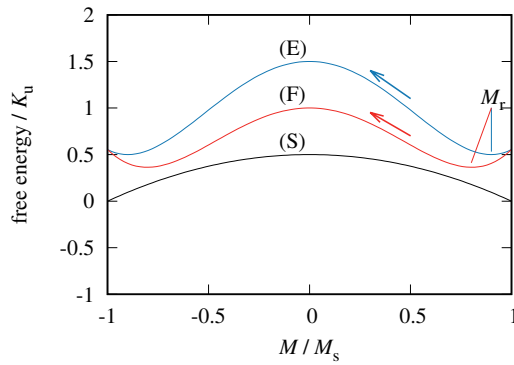
Fig. 3 Energy landscape consisting of internal energy and entropy densities. (E) shows the internal energy density given by eq.(10), (S) shows the entropy density given by eq.(18), and (F) represents the free energy density given by (F)=(E)−(S).

and it tends to increase as the subdivision of magnetic domains becomes small in the multi-domain structure. Consequently, the entropy that can be obtained is

$$S = \ln(P(M)) = -\phi \frac{M^2}{M_s^2} + \phi' \tag{18}$$

where $\phi' = \phi + \ln(\sqrt{\phi/\pi})$. It was found that the entropy of strong anisotropy system is a quadratic function of the order parameter M. The specific free energy density is expressed by Eq. (10), with a multi-domain structure. That is,

$$f(M) = \frac{K_u}{\sigma^4 M_s^4} M^4 - \left(\frac{2K_u}{\sigma^2 M_s^2} - \frac{k_B T \phi}{V M_s^2} - \frac{N_d}{2} \right) M^2 + K_u - \frac{k_B T \phi'}{V} \tag{19}$$

As the free energy landscape has been determined, the coercivity is calculated from the slope of such a function. Now, the order parameter that gives the inflection point is

$$M_c^2 = \frac{\sigma^4 M_s^4}{6 K_u} \left(\frac{2K_u}{\sigma^2 M_s^2} - \frac{k_B T \phi}{V M_s^2} - \frac{N_d}{2} \right) \tag{20}$$

Substituting this value for the slope of the free energy landscape gives,

$$\left(\frac{\partial f}{\partial M} \right)_{M=M_c} = 2M_c \left[\frac{2K_u}{\sigma^4 M_s^4} M_c^2 - \left(\frac{2K_u}{\sigma^2 M_s^2} - \frac{k_B T \phi}{V M_s^2} - \frac{N_d}{2} \right) \right]$$

$$-H_c = -\frac{4\sigma^2 M_s^2}{3\sqrt{6K_u}} \sqrt{\left(\frac{2K_u}{\sigma^2 M_s^2} - \frac{k_B T \phi}{V M_s^2} - \frac{N_d}{2} \right)^3} \tag{21}$$

The temperature dependence of the coercivity H_c was obtained as shown. The entropy effect is schematically shown in Fig.3. (E) is the magnetic energy density, and is depicted as an energy landscape that provides a stable state of magnetization with a squareness of $\sigma = 0.9$. (S) is the functional form of Eq. (18) in term of entropy density. (F) is the energy landscape obtained by subtracting (S) from (E) with the free energy density and using the formula of $F = E - TS$, the figure is displayed with $T = 1$. Owing to the effect of entropy, the energy stabilization point that causes

the residual magnetization M_r has shifted toward $M = 0$. It can also be observed that the slope of the energy landscape indicated by the arrow is also reduced in (F) compared to that in (E). This decrease in inclination represents a decrease in coercivity owing to the entropy effect.

The constants that appear in Eq. (21) in terms of coercivity shows a functional form of $H_c \sim \sqrt{(1 - \gamma T)^3}$ where γ is a constant coefficient. The coercivity, as indicated by Eq. (21) matches with that in Eq. (12) when $T = 0$ and is approximately $H_c \sim \alpha H_k$. Therefore, for the sake of simplicity, $N_d = 0$ was set, and the temperature dependence of H_c was estimated using the parameter α as a function of temperature[*3].

Let us now discuss the Landau theory of ferromagnetic and paramagnetic secondary phase transitions for a localized magnetic moment, m, which is slightly different from the discussion of multi-domain structures. As for the relationship between the order parameter m and the energy landscape, the minimum condition of the free energy corresponds to the stable state of the average magnetic moment, as in the discussion so far. Therefore, the Landau-style phase transition theory defines the internal energy as $E = am^4 + bm^2$ and uses the coefficients a and b as a function of temperature. In this case, the order parameter was normalized to $0 \leq m \leq 1$. Here, the free energy F is defined as $F = E - TS$ and the stable state of the average magnetic moment is analyzed. For example, a ferromagnetic state without fluctuation of magnetization is realized at $m = 1$ at $T = 0$, owing to the settings of $a = 1$ and $b = -2$ on the free energy functions. Using Eq. (18) as the entropy term

$$F = m^4 - (2 - \phi T)m^2 \tag{22}$$

it is possible to investigate the effect of temperature to find the minimum conditions in such free energy. Strictly speaking, the entropy of Eq. (18) considers only the positive and negative value of the magnetization M, so it is an expression corresponding to the Ising model. This is different from the expression of the Heisenberg model that uses the classical localized magnetic moment. However, the main purpose of this study is to analyze a model in which the magnetic domain structure is composed of a larger magnetization array under strong anisotropy. In the analysis of permanent magnets, the directions of magnetic moment are limited by strong magnetic anisotropy as in Ising model, and thus, we decided to carry out this simple analysis to confirm the entropy effect phenomenologically. The average value of the total magnetic moment is approximately $m = 0.8$ when $T = T_c/2$, according to the estimation using the Langevin function. Therefore, by estimating ϕT assuming that $(\partial F/\partial m) = 0$ is realized under the condition of $m = 0.8$, it can be obtained as $\phi T_c/2 = 0.72$.


[*3] The coercivity dependence of $T^{3/2}$ is due to the quartic function representing the free energy landscape. Therefore, when the order of the function changes, the exponent of the power function with respect to the temperature T also changes.

Fig. 4 Energy landscape measurement from magnetization curves. (A) a major loop forming the reference of magnetic energy, (B) a minor loop due to energy excitation. A hatched area between (A) and (B) corresponding to exitation energy by an applied field.

From the result of comparing F with $\sqrt{(1-\gamma T)^3}$, it is considered that the coefficients ϕT and γT are equivalent in the natural unit system because both F and $\sqrt{(1-\gamma T)^3}$ are a normalized. Therefore, considering $\phi T_c/2 = \gamma T_c/2$, the coefficient became $\alpha = 0.593/(3\sqrt{3}\sigma)$ at $T = T_c/2$. In general, the fluctuation of the classical spin by the Langevin function tends to be overestimated in low temperature range. Considering this fact, the decrease in coercivity at a finite temperature is large, and it is considered that entropy is a major cause of the decrease in parameter α in the Kronmüller formula. As previously mentioned, the coefficient ϕ of the entropy term depends on the magnetization process. It should be noted that experimental measurements are required to determine the exact temperature dependence of α. This is because the effect of temperature T on the coercivity is suppressed if $\phi \ll 1$. In this sense, the reduction factor α in the Kromüller formula is governed by the change in entropy S with respect to the change in the magnetization state M. If this change in entropy can be suppressed, coercivity may increase even at higher temperature. Furthermore, it is presumed that the temperature dependence of the coercivity is different even for a similar composition of permanent magnet materials, which can be explained by the difference in the magnetic entropy due to the influence of the crystal texture.

4 Analysis of free energy landscape including temperature and entropy effects

4.1 Measurement of free energy landscape

To analyze the coercivity, it is necessary to find the free energy landscape as a function of the order parameter M. To analyze the coercivity, as shown by Eq. (3), the influence of the external magnetic field is compared with the slope of landscape. Therefore, it is necessary for the order parameter in the function of the free energy landscape not to be influenced by the external field. The procedure for this measurement is illustrated in Fig.4. The magnetization curve of (A) shows part of a major loop, where measurements begin with an external magnetic field $+H_s$ that saturates the magnetization and passes through the remanent state $M_r(H = 0)$ and the coercivity state $-H_c$. Finally, magnetization reversal occurs. In contrast, the magnetization curve of (B) is a minor loop under the external magnetic field condition $H_i \to H = 0$. To obtain (B), the measurement is started from $+H_s$, passes through $H = 0$, and then the magnetic field sweep is reversed at H_i that satisfies the condition $0 > H_i > -H_c$. Here, the magnetization state obtained from the external magnetic field condition of H_i is defined by the intersection of the minor loop (B) and $H = 0$, and is defined as M_i. This magnetic measurement procedure is similar to the FORC (First-Order Reversal Cureve) analysis. Focusing on the condition of $H = 0$ in Fig.4 regarding the magnetization state of magnetic materials, the order parameter was relaxed from M_r to M_i. This relaxation process is due to the energy increase corresponding to the area Δ_i surrounded by
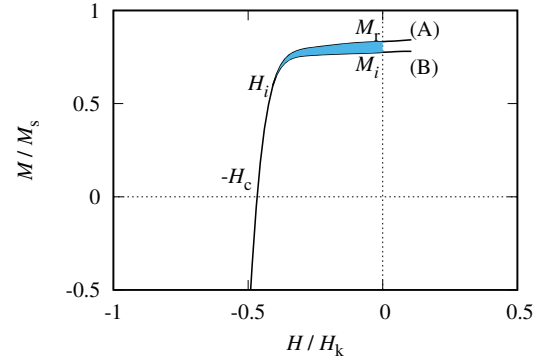
the area $M_r - H_i - M_i$ (gray hatch) between the major loop (A) and minor loop (B). In Fig. 2 shown as an example of energy landscape, the decrease in magnetization in the region of $M > 0$ corresponds to the process of increasing energy due to work from outside of the system. The Helmhortz-type free energy used in Landau theory describes an open system. That is, it can be seen that the magnetization state is destabilized by the excitation energy from the outside in the process of magnetization reversal, and the magnetization is relaxed. Because the decrease in magnetization corresponds to the decrease in the order parameter, it is expressed that the magnetization of the system is relaxed. Therefore, based on the M_r state, the free energy density corresponding to the order parameter M_i is

$$f(M_i) = f(M_r) + \Delta_i \qquad (23)$$

In Eq. (23), $f(M_i)$ is uniquely determined by Δ_i; the free energy landscape $f(M_i)$ can be obtained, where a series of magnetization $M_r > \cdots > M_{i-1} > M_i > M_{i+1} > \cdots > 0$ are measured under the conditions of the external magnetic fields $0 > \cdots > H_{i-1} > H_i > H_{i+1} > \cdots > -H_c$.

4.2 Separation of entropy terms

The free energy density determined by the measurements shown in Fig.4 should be in the form of Eq. (15). Here, to enable a detailed discussion of the energy landscape analysis, we attempt to separate the entropy term from the measurement results. Two curves $f^j(M)$ and $f^{j+1}(M)$ representing the free energy landscape are obtained by measuring Fig.4 under two different temperature conditions, $:0 < T_j < T_{j+1} < T_c$. As the function $\varepsilon(M)$ in Eq. (15) is independent of the conditions T_j and T_{j+1},

$$\frac{f^j(M) - f^{j+1}(M)}{k_B \delta T} = -\frac{S(M)}{V} \qquad (24)$$

The entropy density of the system can be determined as above, where $\delta T = T_j - T_{j+1}$. Moreover, because the limit of $\delta T \to 0$

matches the definition formula of entropy density, it can be measured without change in the global magnetic domain structure due to the thermal fluctuation of magnetization, if the difference between T_j and T_{j+1} is reduced. Using the free energy landscape f determined using Eq. (23) and the S obtained by Eq. (24), the function form is obtained in

$$f^j(M) = \varepsilon(M) - \frac{k_B T_j S(M)}{V} \tag{25}$$

The internal energy density of the system ε can also be described as above. The identification of ε is important for understanding the coercivity mechanism, and it should also be considered that the barrier height of the energy landscape may not necessarily match K_u depending on the magnetization process. To improve the measurement accuracy of the energy landscape, we increased the measurement point T_j to ensure statistical reliability.

5 Summary

This study attempted to derive the Kronmüller formula by conducting an analysis within the framework of the Ginzburg-Landau theory. The results showed that the coercivity of the magnetic material was defined by the slope of the free energy landscape. The reduction parameter α for the magnetic anisotropy field H_k in the Kronmüller formula depends on the functional form representing the free energy landscape that changes with the magnetization process of the material, and it is shown that $\alpha < 1$ even under the condition of absolute zero temperature $T = 0$. Furthermore, α depends on the entropy of the system and it may show a larger reduction rate at a finite temperature $T \neq 0$. Thus, it is important to acquire the free energy landscape and clarify the order parameter dependence of entropy in the magnetization process of the magnetic material.

This study does not explicitly include the interactions owing to the spatial distribution of magnetization. For example, to incorporate the effect of the domain wall as internal energy, it is necessary to introduce the term of $A(\nabla M)^2$. Here, A is the exchange stiffness constant and ∇M is the spatial derivative of the magnetization. However, to incorporate specifically the domain wall shape into the framework of the Ginzburg-Landau theory, it is necessary to introduce a functional representation or quantification of the magnetic domain structure. This theory needs to be extended to capture the effects of spatial modulation associated with the magnetization distribution [9,10], including a more accurate representation of the magnetic dipole interactions.

References

1) H. Kronmüller: *Phys. Stat. Sol. (b)* **144** , 385 (1987).
2) H. Kronmüller and K.-D. Durst: *J. Magn. Magn. Mater.* **74**, 291 (1988)
3) S. Hirosawa, K. Tokuhara, S. Mino, T. Matsui, K. Morii and Y. Nakayama: *MRS Sym. Proc.* **232**, 275 (1991).
4) L. D. Landau and E. M. Lifshitz: "Statistical Physics" (Pergamon, Oxford,1980)
5) K. Iwano, C. Mitsumata, and K. Ono: *J. Appl. Phys.* **115**, 17D134 (2014).
6) K. Iwano, C. Mitsumata, and K. Ono: *J. Appl. Phys.* **117**, 17A704 (2015).
7) K. Iwano, C. Mitsumata and K. Ono: *J. Phys. Soc. Jpn.* **85**, 074711 (2016).
8) Y. Toga, S. Miyashita, A. Sakuma and T. Miyake: *npj Computational Materials*, **6**, 67 (2020).
9) A. L. Foggiatto, S. Kunii, C. Mitsumata, and M. Kotsugi: To be submitted
10) K. Masuzawa, S. Kunii, A. L. Foggiatto, C. Mitsumata, and M. Kotsugi: *T. Magn. Soc. Jpn. (Special Issues)* **6**, 1 (2022)
11) Y. Matsuura; *40th. Ann. meeting of Magn. Soc. Jpn*, 7aE-6 (2016)

<Paper>

Magnetocardiography Inverse Estimation from a Realistic Ventricular Model Using Spatial Filter Methods: A Simulation Study

Wenxu Sun, Morio Iwai*, Koichiro Kobayashi*

Faculty of Engineering, Kindai Univ., *1-Umenobe, Takaya, Higashi-Hiroshima, Hiroshima 739-2116, Japan*

* Faculty of Science and Engineering, Iwate Univ., *4-3-5 Ueda, Morioka, Iwate 020-8551, Japan*

We used a lead field normalization and measurement covariance matrix R into a weighted minimum-variance spatial filter (WMV). An inverse estimation, with an extended source, arranged at the surface of a realistic ventricular model was carried by WMV, weight-normalized minimum-norm (WMN), and minimum-variance spatial filter (MV) with and without noise. The performances of these spatial filters were evaluated using the estimation error and ratios of all positions with an estimation error below 2 cm. Moreover, the proper regularization parameter was determined from the estimation error. The results of the statistical analysis, while handling varied source positions, show that WMV has the best performance for magnetocardiography (MCG) extended source inverse estimation because it leads to less estimation error and is capable of stable inverse estimation, even at high noise levels. In other words, the combined lead field normalization, with the measurement covariance matrix R used in WMV, is a good choice for our MCG system.

Key words: Magnetocardiography, inverse estimation, source localization, spatial filter

1. Introduction

Despite being fatal, frequent premature ventricular contraction (PVC) is treated with catheter ablation to improve the patient's quality of life. During ablation, 3D electro-anatomical mapping is used to precisely locate the origin [1]; however, some non-invasive techniques are required to locate the origin. Relatively uniform magnetic permeability enables magnetocardiography (MCG) to yield higher spatial resolution of inverse estimation of the origin compared with electrocardiography [2]. To solve the ill-posed bioelectromagnetic inverse problem, spatial filtering techniques are widely used.

One prominent class of techniques, known as non-adaptive spatial filters, including the original minimum-norm method (MN), weight-normalized minimum-norm method (WMN) method, and low-resolution electromagnetic tomography (LORETA) [3]-[5]. MN tends to concentrate the solution near the surface, regardless of the true depth of the source. This is because the sensitivity of the sensor decays rapidly with depth. The tendency to concentrate the solution at the surface can be overcome by introducing proper depth weighting [4]. Lead field normalization is effective in compensating for the varied sensitivities of the sensors to the current sources at different depths [6]-[7]. Another popular class is the adaptive spatial filter, which introduces the covariance matrix of the measurements. A well-known example of this class is the minimum-variance spatial filter (MV) [8]-[9]. Sekihara et al. reported that MV exhibits bias in the reconstructed location of a single source;

however, this bias can be eliminated using the normalized lead field [10]. In this study, lead field normalization is used in MV, which is called the weighted minimum-variance spatial filter (WMV).

Equivalent current dipole and distributed source models are usually used for MEG/EEG source localization [11]-[13]. An extended source may be suitable for the prior estimation of PVC origin in MCG studies, according to the clinical reports of catheter ablation. Moreover, a proper solution space needs to be determined. In our previous study [14]-[15], an unconstrained solution space, with thousands of voxels that covered the human heart, was used for MCG source localization, which resulted in the appearance of an unexpected solution. In this study, a realistic ventricular model was used as the allowable solution space. An extended source was arranged at the surface of the ventricular model that represented the endocardium and epicardium. Despite the origin of PVC in the myocardium, the excitement can propagate into the endocardium or epicardium rapidly. Hence, the source was constrained at the surface of the ventricle.

In this study, we aim to evaluate the accuracies of the inverse estimation using the WMN, MV, and WMV methods based on an extended source and a realistic ventricular model.

2. Methods

2.1 Source Model and MCG System

A realistic ventricular model, reported in our previous study [16], was generated from computed tomography images. A total of 530 nodes and 1064 faces were generated at the surface of the ventricular model using the iso2mesh toolbox [17]. Magnetic fields were simulated to arise from an extended (about 1 cm) current source that contains a center and 4–7 neighbor nodes. Because

Corresponding author: Wenxu Sun
(e-mail: wxusun@gmail.com).

the excitement propagates along the surface and across the ventricular myocardial, two dipoles in the tangential and normal directions are arranged in each neighbor node. The MCG planar sensor array contains 64 channels of the first-order gradiometer with a baseline of 5 cm. The sensors are arranged in an 8 × 8 matrix with 25 mm pitch and a 175 × 175 mm measurement area (Fig. 1).
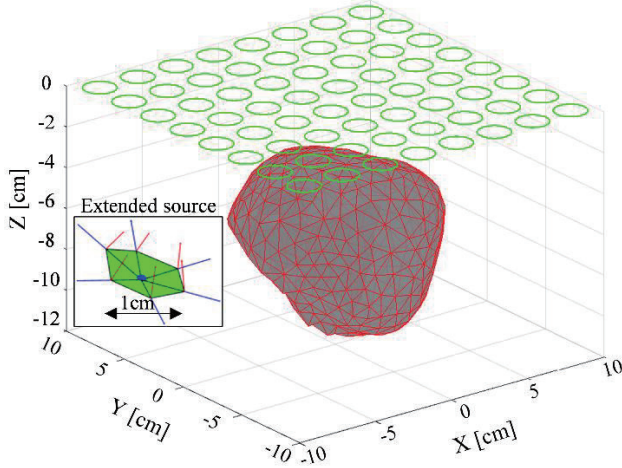

Fig. 1. MCG system and source model.

Because the MCG inverse problem is ill-posed, weak noise signals can cause large changes in the solution. In this study, Gaussian white noise was added to the simulated magnetic field data, and the inverse solutions were computed using the above three spatial filters. The signal-to-noise ratio (SNR) ranges from 0 to 40 in 10 dB increments. The SNR is defined as

$$\text{SNR} = 10 \log \frac{\text{var}(\boldsymbol{B}_{\text{exact}})}{\sigma^2}, \tag{1}$$

where $\boldsymbol{B}_{\text{exact}}$ is the variance of the simulated noise-free measurements, and σ^2 is the variance of the added Gaussian white noise.

2.2 Spatial Filters

The basic function of bio-magnetic forward problem is given by

$$\boldsymbol{B} = \boldsymbol{K}\boldsymbol{J} + \boldsymbol{n}, \tag{2}$$

where $\boldsymbol{B}$ is the vector of measured signals; $\boldsymbol{K}$ is the sensor lead field matrix and can be obtained from the Biot–Savart Law; $\boldsymbol{J}$ is the original current sources within the heart, and $\boldsymbol{n}$ is the additive noise. The estimated current sources $\hat{\boldsymbol{J}}$ can be estimated by a simple linear operator, as follows.

$$\hat{\boldsymbol{J}} = \boldsymbol{T}\boldsymbol{B}. \tag{3}$$

Here, $\boldsymbol{T}$ is the spatial filter matrix (i.e., inverse operator). For the well-known MN method, the estimated current sources can be written as

$$\hat{\boldsymbol{J}} = \boldsymbol{K}^{\text{T}}(\boldsymbol{K}\boldsymbol{K}^{\text{T}} + \lambda^2 \boldsymbol{I})^{-1}\boldsymbol{B}, \tag{4}$$

where T denotes the matrix transpose, λ^2 is the regularization parameter, and $\boldsymbol{I}$ is the identity matrix.

The MV spatial filter is a representative adaptive spatial filter that introduces the measurement covariance matrix $\boldsymbol{R}$. The estimated current sources can be written as

$$\hat{\boldsymbol{J}} = \frac{\boldsymbol{K}^{\text{T}}\boldsymbol{R}^{-1}}{\boldsymbol{K}^{\text{T}}\boldsymbol{R}^{-1}\boldsymbol{K}}\boldsymbol{B}. \tag{5}$$

For bio-magnetic inverse estimation, lead field normalization is usually used to compensate for the varied sensitivity and modify the corresponding columns of $\boldsymbol{K}$, to make the sensitivity the same for all locations $\boldsymbol{r}$. Hence, the WMN spatial filter can be expressed as

$$\hat{\boldsymbol{J}} = \widetilde{\boldsymbol{K}}^{\text{T}}(\widetilde{\boldsymbol{K}}\widetilde{\boldsymbol{K}}^{\text{T}} + \lambda^2 \boldsymbol{I})^{-1}\boldsymbol{B}, \tag{6}$$

where $\widetilde{\boldsymbol{K}}$ is the normalized lead field matrix [10].

The WMV spatial filter method and can expressed as

$$\hat{\boldsymbol{J}} = \frac{\widetilde{\boldsymbol{K}}^{\text{T}}\boldsymbol{R}^{-1}}{\widetilde{\boldsymbol{K}}^{\text{T}}\boldsymbol{R}^{-1}\widetilde{\boldsymbol{K}}}\boldsymbol{B}. \tag{7}$$

2.3 Statistical Analysis

The source positions were varied within the surface of the ventricular model, and the MCG simulation and inverse estimation were repeated with different added noise levels. The estimation error was the distance between the position of the center node of the extended source and the estimated result (Fig. 2). In this study, an estimation error of less than 2 cm is considered an effective prediction. Hence, the ratios of all positions with an estimation error below 2 cm were used to evaluate the accuracy of inverse estimation using the three types of spatial filters.
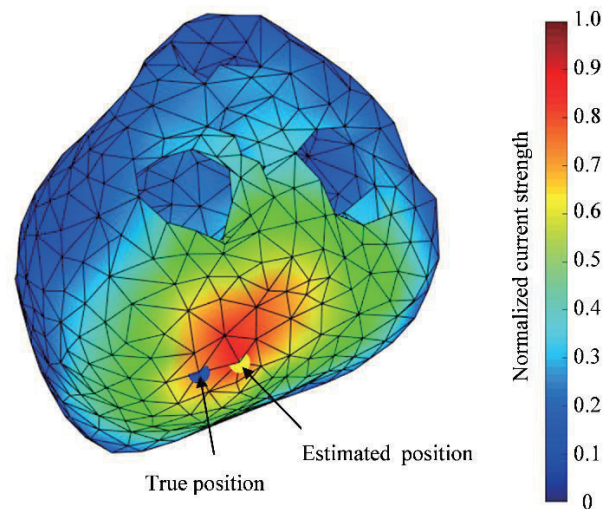

Fig. 2. Definition of estimation error.

3. Results

Fig. 3 shows the noise free estimation results of the true position at node index 6 (Fig. 3 (a)) and 437 (Fig. 3 (b)), respectively. The blue point indicates the true position of the center node of the extended source. The yellow point indicates the position of the estimated maximum current strength. The three types of spatial filters can estimate the source position with high accuracy for node index 437, which is near the sensors. However, for a relatively deep node, such as node 6, which is far from the sensors, the WMN tends to concentrate the solution in a shallow position, leading to a relatively large spatial extension. In contrast, MV and WMV spatial filters can both estimate the source position with high accuracy and spatial resolution.

Generally, the regularization parameter λ^2 is introduced to solve the ill-posed problem. The proper value of λ^2 is usually determined by the L-curve method [18]. In this study, we evaluated the mean estimation error through statistical analysis at varied regularization parameters to determine the proper value. In addition, the regularization parameter λ^2 can be evaluated by the product of constant a and the sum of all elements in matrix $\boldsymbol{KK^T}$. Fig. 4 shows that the estimation error depended on constant a. The proper constants a of WMN are 1.0×10^{-9} without noise, and 1.0×10^{-5}, 1.0×10^{-4}, 1.0×10^{-3}, and 1.0×10^{-2} for noise levels of 40, 30, 20, and 10 dB. However, a relatively large constant ($a = 1$) would lead to a low spatial resolution, despite showing higher accuracy than $a = 0.1$. a seems to be stable below 0.001 and 0.01 for MV and WMV, respectively. Hence, in this study, inverse estimation was performed with varied a values at different noise levels for WMN. Moreover, $a = 0.001$ was used for MV and WMV for the entire experiment.

In the simulation experiment, the source positions were varied within the surface of the ventricular model, and the inverse estimation was repeated 530 times at each noise level. The results of statistical analysis are shown in Fig. 5. Fig. 5 (a) and (b) indicate the mean values of the estimation error and ratios of all positions with an estimation error below 2 cm at different levels,
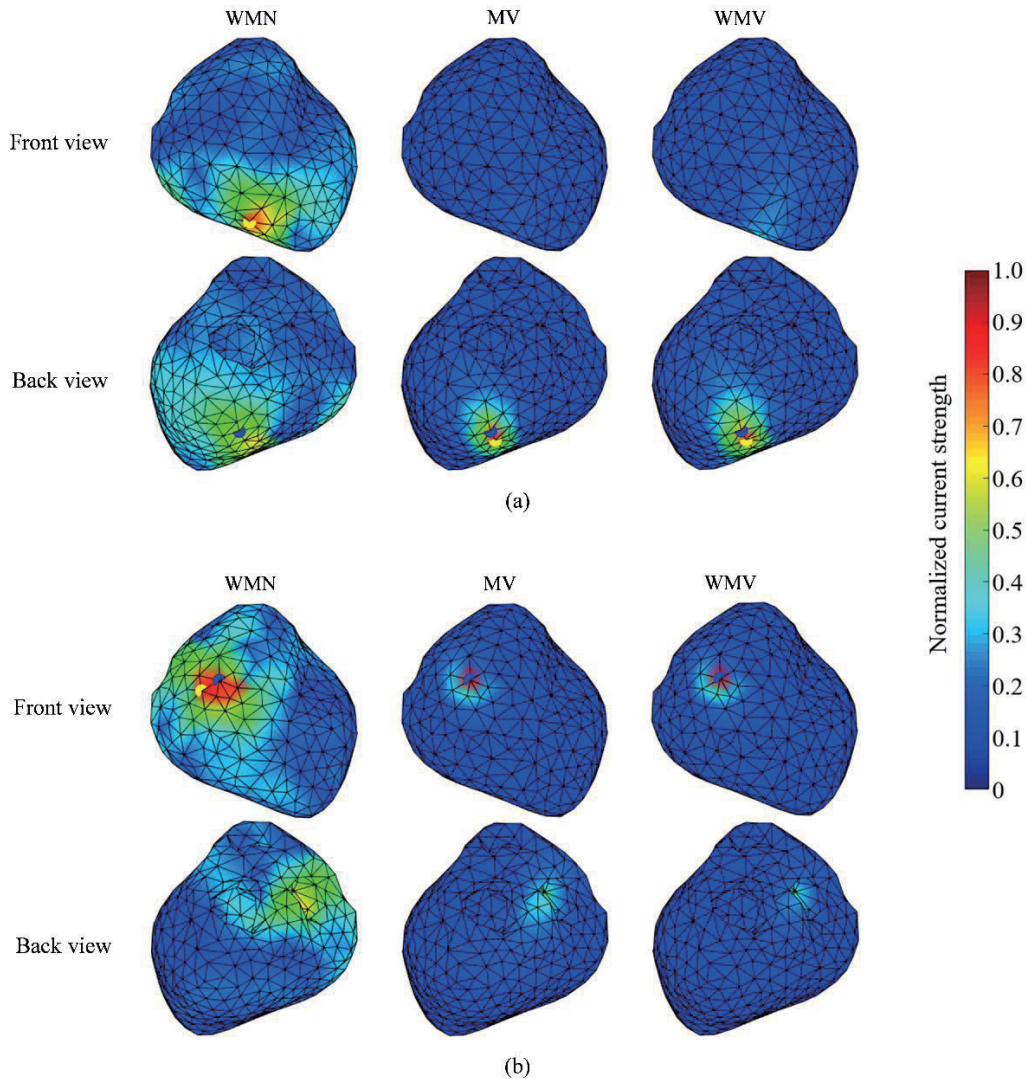

Fig. 3. Estimation results of the true source located at (a) node 6 and (b) node 437 without noise.

respectively. For a relatively low noise level (SNR = 40 dB), MV and WMV have 83% (MV), and 88% of all positions with an estimation error below 2 cm. Additionally, the mean values of the estimation error of MV and WMV are 1.0 and 0.8 cm, respectively. However, the ratio of all positions with an estimation error below 2 cm was only 67% and the mean value of the estimation error was 2.1 cm for the WMN spatial filter. Conversely,
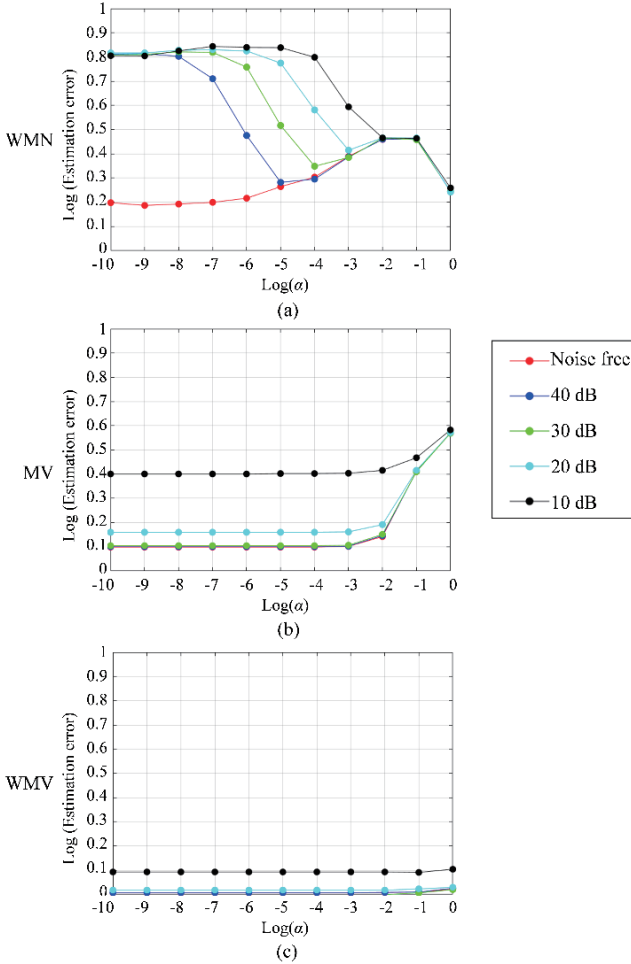
under the condition of high noise level (SNR = 10~20 dB), the accuracies of MV decreased rapidly, but WMV

(a)

(b)

(c)

Fig. 4. Estimation error with different constant α.

(a)

(b)
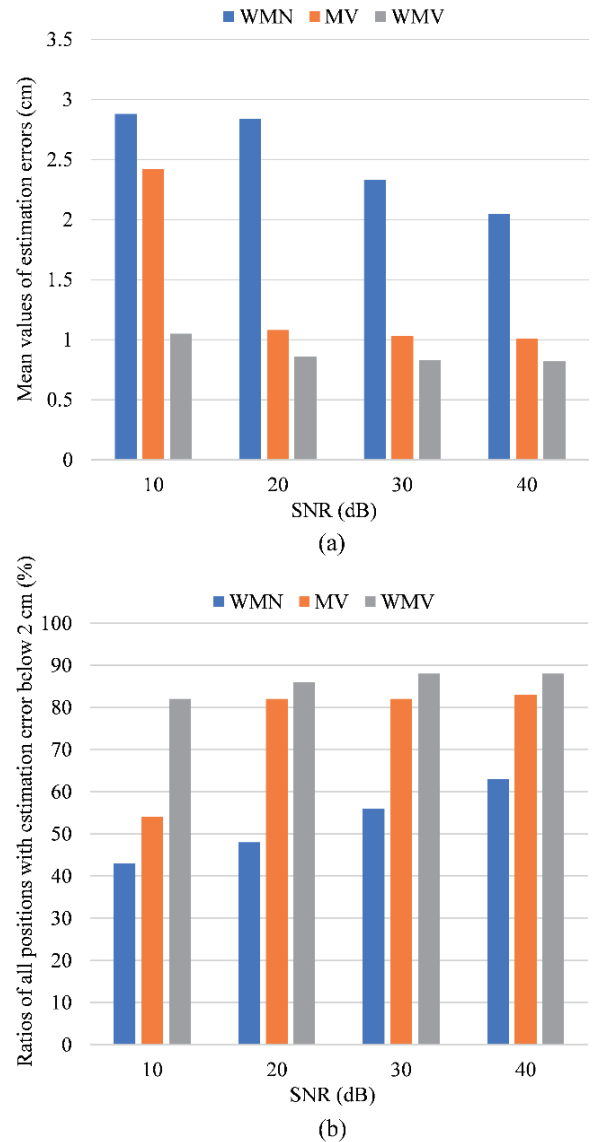
Fig. 5. Statistical analysis results.
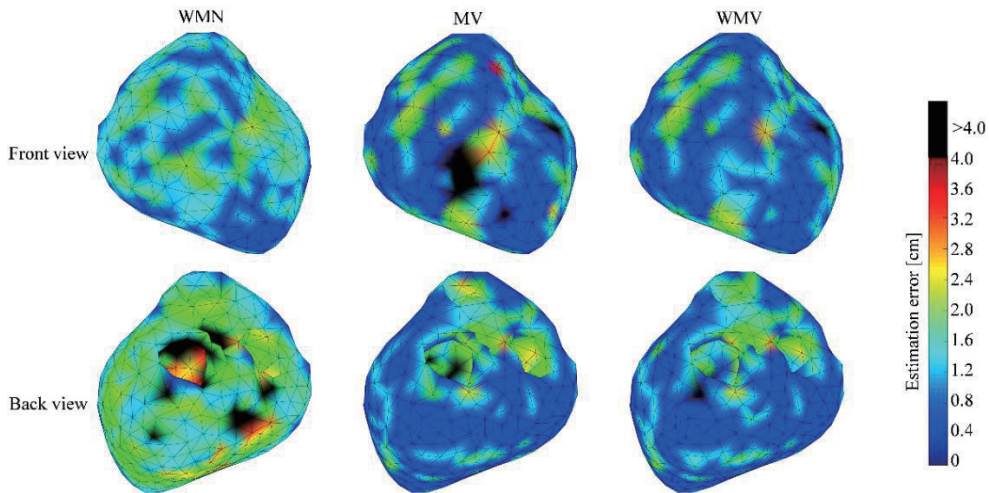
Fig. 6. Distribution of estimation error without noise.

appeared stable. The mean value of the estimation error was 1.1 cm, and more than 80% of all positions had an estimation error below 2 cm for WMV at 10 dB. Thus, MV demonstrated stable accuracy at 20~40 dB. Furthermore, the WMV method achieved the best performance in this study.

4. Discussion

In this study, we evaluated the proper regularization parameters by assessing the estimation error with different constants a for the WMN, MV, and WMV spatial methods. Then, the mean value of the estimation error and the ratios of all positions with an estimation error below 2 cm were used to evaluate the performance of the three types of spatial filters. MV and WMV showed that they could estimate the source position with higher accuracy than WMN. This is probably a result of using the measurement covariance matrix R in the inverse estimation procedure. Because the noise level is different in every sensor, the introduction of the measurement covariance matrix R into the inverse estimation can also enhance the stability of accuracy at different noise levels. Fig. 6 shows the distribution of the estimation error for WMN, MV, and WMV without noise. WMN cannot estimate the source located far from the sensors. In contrast, MV shows some areas near the sensors with low accuracy. However, lead field normalization has solved these problems in WMV. In other words, combining lead field normalization with the measurement covariance matrix R, which is used in WMV, is advantageous for our MCG system.

5. Conclusion

In this study, inverse source estimation from a simulated MCG with an extended source is conducted in a realistic ventricular model using WMN, MV, and WMV spatial filters. The performances of the three spatial filters are evaluated with and without noise. The results of the statistical analysis handling varied source positions show that WMV has the best performance for MCG source inverse estimation. In the future, the effectiveness of WMV method will be investigated by using the clinical MCG data obtained from PVC subject who was ablated successfully.

References

1) Morady F, et al.: *Circulation*, **82**, 2093 (1990).
2) Kirsten Tolstrup, et al.: *Cardiology*, **106**, 270 (2006).
3) Leahy RM, et al.: *Electroencephalogr. clin. Neurophysiol*, **107**, 159 (1998).
4) Sunao Iwaki and Shoogo Ueno: *J. Appl. Phys.*, **83**, 6441 (1998).
5) Pascual-Marqui, R. D: *Int. J. bioelectromagn.*, **1**, 75 (1999).
6) Grech, R, et al.: *J. NeuroEng. Rehabil.*, **5**, 25 (2008).
7) Tamesh Halder, et al.: *eNeuro.*, **6**, 0170 (2019).
8) B. D. Van Veen, et al.: *IEEE Trans. Biomed. Eng.*, **44**, 867 (1997).
9) Fernández-Corazza M, et al.: *Int. J. Numer. Method Biomed. Eng.*, **31**, 2 (2015).
10) Kensuke Sekihara, et al.: *NeuroImage*, **25**, 1056 (2005).
11) Rupali P. Dhond, et al.: *J. Altern. Complem. Med.*, **14**, 679 (2008).
12) Keith S. Cover, et al.: *Int. Cong. Series*, **1300**, 121 (2007).
13) Kiebel SJ, et al.: *Neuroimage*, **39**, 728 (2008).
14) W. Sun and K. Kobayashi: *IEEE Trans. Mag.*, **53**, 1 (2017).
15) W. Sun and K. Kobayashi: *J. Magn. Soc. Jpn.*, **41**, 75 (2017).
16) Takashi Ijiri, et al.: *PLoS ONE*, **7**, e36706 (2012).
17) Qianqian Fang and David Boas: *Proc. ISBI*, 1142 (2009).
18) Per Christian Hansen and Dianne Prost O'Leary; *SIAM J. Sci. Comput.*, **14**, 1487 (1993).

Notice for Photocopying

If you wish to photocopy any work of this publication, you have to get permission from the following organization to which licensing of copyright clearance is delegated by the copyright owner.

〈All users except those in USA〉
Japan Academic Association for Copyright Clearance, Inc. 〔JAACC〕
6–41 Akasaka 9-chome, Minato-ku, Tokyo 107–0052 Japan
Phone 81–3–3475–5618　FAX 81–3–3475–5619　E-mail: info@jaacc.jp

〈Users in USA〉
Copyright Clearance Center, Inc.
222 Rosewood Drive, Danvers, MA01923 USA
Phone 1–978–750–8400　FAX 1–978–646–8600

複写をされる方へ

当学会は下記協会に複写複製および転載複製に係る権利委託をしています．当該利用をご希望の方は，学術著作権協会（https://www.jaacc.org/）が提供している複製利用許諾システムもしくは転載許諾システムを通じて申請ください．ただし，本誌掲載記事の執筆者が転載利用の申請をされる場合には，当学会に直接お問い合わせください．当学会に直接ご申請いただくことで無償で転載利用いただくことが可能です．

権利委託先：一般社団法人学術著作権協会
　　　　　　〒107–0052 東京都港区赤坂9-6–41　乃木坂ビル
　　　　　　電話（03）3475-5618　FAX（03）3475-5619　E-mail: info@jaacc.jp